

MAC-XA: Multi-view Anatomy-Correspondence Fusion for Coronary Stenosis Reporting from X-ray Angiography

Chen Jia^{1,6}, Baochang Zhang^{1,2,3*}, Fatia Kusuma Dewi¹, Amir Yousefi¹,
Heribert Schunkert^{2,4}, Reza Ghotbi⁵, and Nassir Navab^{1,3}

¹ Computer Aided Medical Procedures, Technical University of Munich, Munich, Germany

{chen.jia,baochang.zhang}@tum.de

² German Heart Center Munich, Munich, Germany

³ Munich Center for Machine Learning, Munich, Germany

⁴ German Centre for Cardiovascular Research, Munich Heart Alliance, Munich, Germany

⁵ HELIOS Hospital West of Munich, Munich, Germany

⁶ relAI – Konrad Zuse School of Excellence in Reliable AI, Munich, Germany

Abstract. Multi-view reasoning in coronary X-ray angiography is inherently a cross-projection geometric problem, yet automated report generation in this setting remains largely unexplored. The 3D vascular topology leads to projection-dependent branch overlap and foreshortening, rendering single-view modeling fundamentally incomplete and unstable for lesion localization and stenosis grading. Although multi-view fusion appears promising, learning anatomically consistent fusion from real angiograms is impeded by a critical limitation: cross-view alignment is unobservable and cannot be explicitly supervised. Consequently, conventional fusion relies on implicit correlations rather than verified anatomical correspondence. We address this by reformulating multi-view stenosis reporting as an alignment-constrained aggregation problem. A controllable synthetic angiography generation strategy is introduced to expose geometry-derived patch-level correspondence supervision unavailable in real data. An anatomy-correspondence module learns cross-view correspondence matrices that explicitly align auxiliary features within the main-view coordinate space prior to fusion, thereby constraining evidence aggregation to anatomically consistent regions. Experiments on synthetic data and zero-shot transfer to real angiograms show that this alignment-constrained design improves correspondence consistency and structured stenosis reporting compared to single-view modeling and conventional multi-view fusion methods. The code will be publicly available upon publication.

Keywords: Medical Report Generation · Coronary Stenosis Reporting · Anatomy-Correspondence Fusion · Multi-view X-ray Angiography.

* Corresponding author.

1 Introduction

Coronary artery stenosis is a major driver of coronary artery disease and requires precise localization and grading [1, 13]. Projection-based X-ray imaging compresses 3D anatomy into a 2D plane, removing depth cues and introducing view-dependent distortion [6, 15]. In coronary angiography, thin vessels, uneven contrast, and device interference further exacerbate projection-induced branch overlap and foreshortening, causing lesion visibility to vary substantially across views [3, 18]. Near vascular bifurcations, similar local appearance combined with frequent overlap makes single-view branch identification particularly unreliable [9, 5, 7]. Reliable stenosis reporting therefore requires integrating evidence across projections and reasoning over consistent vascular topology. Despite this clinical reality, automated multi-view report generation in coronary angiography remains largely underexplored.

Related work has explored multi-view report generation and fusion mainly in chest X-ray settings, typically fusing images via attention or contrastive objectives and learning cross-view interactions implicitly from the end-task loss. For example, multi-view contrastive learning can strengthen representations and provide auxiliary guidance for transformer decoding [2, 10]. Other frameworks first derive prior concepts and then decode reports from fused multi-view knowledge [11]. More generally, multi-view fusion designs such as Duoduo CLIP [8] aggregate features with cross-view attention on top of CLIP-like encoders. Despite their progress, these approaches rarely enforce verifiable anatomical correspondence across projections. As a result, attention mechanisms may align visually similar but anatomically unrelated regions, leading to unstable cross-view aggregation under strong overlap, large viewpoint changes, or near bifurcations.

In this work, we propose a multi-view anatomy-correspondence fusion framework that explicitly learns cross-view correspondences to guide evidence fusion for coronary stenosis reporting. Our main contributions are: (1) We reformulate multi-view coronary stenosis reporting as an alignment-constrained aggregation problem, highlighting the necessity of explicit cross-view anatomical correspondence in projection-based imaging. (2) To overcome the absence of verifiable alignment supervision in real angiograms, we introduce a controllable synthetic angiography generation strategy that provides geometry-derived patch-level cross-view correspondence ground truth together with structured stenosis reports. (3) We design a correspondence-driven multi-view framework in which predicted cross-view correspondence matrices explicitly align auxiliary features within the main-view coordinate space prior to aggregation, enabling anatomically consistent multi-view reasoning. We validate this design through synthetic evaluation and zero-shot transfer to real angiograms.

2 Method

An overview of the proposed method is illustrated in Fig. 1, comprising Anatomy-Correspondence Module (ACM) pretraining with geometry-derived correspon-

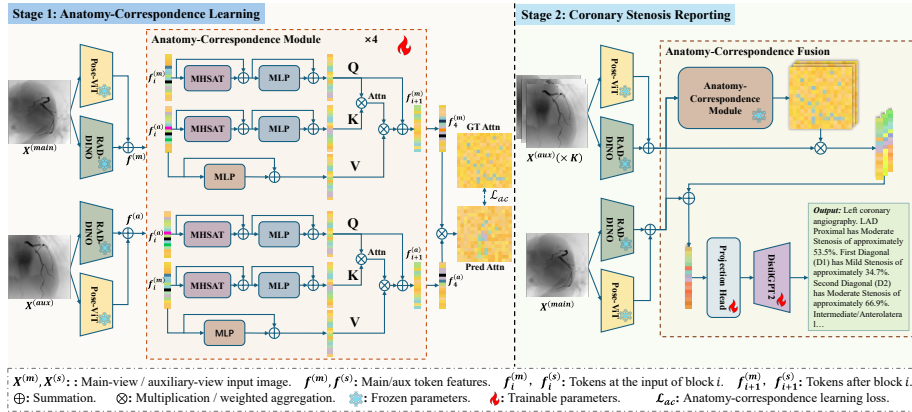


Fig. 1: Overview of MAC-XA. Stage 1 pretrains ACM with geometry-derived correspondence supervision. Stage 2 uses the learned correspondences for multi-view fusion and structured stenosis report generation.

dence supervision and correspondence-guided multi-view fusion for stenosis report generation.

2.1 Problem Reformulation

Single-view stenosis reporting maps one angiography view X to a structured report \mathbf{y} . In practice, however, each case contains multiple views acquired in the same exam. We therefore consider a training set $\mathcal{D}_{tr} = \{(\mathbf{X}_i, \mathbf{y}_i)\}_{i=1}^N$, where i indexes a case, $\mathbf{X}_i = \{X_i^{(v)}\}_{v=1}^{K_i}$ denotes its K_i available views, and \mathbf{y}_i is the corresponding structured report. The goal is to learn a mapping from \mathbf{X}_i to \mathbf{y}_i for each case.

The central challenge is how to fuse evidence across views reliably. To make multi-view fusion anatomically grounded, we introduce cross-view anatomical correspondence as an explicit alignment prior. Each view is encoded into P patch tokens, and for any view pair we estimate a patch-level correspondence matrix supervised by geometry-derived ground truth in the synthetic data. Given a selected main view and one or more auxiliary views, the predicted correspondences are used to align auxiliary features to the main-view patch coordinate space before fusion, so that report generation is based on anatomically matched evidence rather than implicit feature mixing.

2.2 Anatomy-Correspondence Ground Truth Preparation

Fine-grained cross-view anatomical alignment is not directly observable in real coronary angiography. To obtain reliable supervision, we therefore synthesize multi-view X-ray angiograms from real ASOCA 3D CTA volumes [4] and record the view label and projection pose for each rendering. Our pipeline follows a

standard CTA-to-angiography simulation process. Starting from coronary artery extraction, we extract vessel centerlines, reconstruct vessel surfaces, and simulate localized stenoses by applying shape- and severity-controlled narrowings at diverse surface locations. We render 2D digitally reconstructed angiograms (DRRs) via a physics-based projection model [20], producing multi-view projections for both LCA and RCA in each simulated case. To link 3D lesion metadata to clinically meaningful text, we label each 3D centerline branch according to SYNTAX Score segment definitions [17], which enables automatic generation of structured plain-text reports during simulation. Each simulated case is paired with a structured stenosis report containing branch identity, severity grade, and percentage stenosis.

We further construct anatomy-correspondence ground truth (AC-GT) from geometric consistency across known projections. Specifically, we sample 3D points $\{p_n\}$ along the vessel centerlines, project them into each view v using the recorded pose parameters, and map each projected point to a RAD-DINO [14] patch index $\pi^{(v)}(p_n) \in \{1, \dots, P\}$. For any view pair (α, β) , we define a binary patch-to-patch ground-truth correspondence matrix $\mathbf{A}_{\alpha \rightarrow \beta}^{\text{gt}} \in \{0, 1\}^{P \times P}$ by setting $\mathbf{A}_{\alpha \rightarrow \beta}^{\text{gt}}[i, j] = 1$ if there exists a sampled point p_n such that $\pi^{(\alpha)}(p_n) = i$ and $\pi^{(\beta)}(p_n) = j$, and 0 otherwise. If multiple 3D points fall into the same patch in the main view, the corresponding row can contain multiple positive entries in the auxiliary view, reflecting the inherent many-to-many mapping induced by projection. This matrix provides a geometry-derived supervision target for cross-view anatomical consistency at the patch level.

2.3 Anatomy-Correspondence Learning

Pose-aware embedding. Since correspondence must be inferred across views with substantial pose-induced appearance changes, we encode each view $X^{(v)}$ with two frozen encoders. RAD-DINO provides patch tokens $T^{(v)} \in \mathbb{R}^{P \times d}$ (plus a global [CLS] token) for local appearance cues, while a pose-aware encoder (PoseViT, ViT-B/32 pretrained on pose classification) outputs a view embedding $e^{(v)}$ that encodes acquisition pose. We inject $e^{(v)}$ into the [CLS] token to form view-conditioned tokens $f^{(v)} \in \mathbb{R}^{(P+1) \times d}$ for subsequent correspondence learning. For each view pair, the selected main and auxiliary representations are denoted by $f^{(m)}$ and $f^{(a)}$, respectively. These are passed to the ACM, a supervised and inspectable module that stacks four mapping blocks to progressively align the two views.

Bidirectional correspondence reasoning. We model cross-view correspondence by performing correspondence estimation and geometry-aware information transfer in both directions within each mapping block. Specifically, the block consists of two symmetric branches, $m \rightarrow a$ and $a \rightarrow m$, which share parameters by swapping the roles of the main and auxiliary views. Within each branch, we first apply lightweight intra-view token refinement (self-attention followed by an MLP) to both views, and then perform a cross-view attention step: main-view tokens produce queries, while auxiliary-view tokens produce keys and values,

yielding correspondence logits $Z_{m \rightarrow a} \in \mathbb{R}^{(P+1) \times (P+1)}$ and the row-normalized attention weights $G_{m \rightarrow a} = \text{softmax}(Z_{m \rightarrow a})$, which update the main-view tokens via a residual cross-view message.

Correspondence prediction. After the iterative mapping, we compute correspondence logits using dot-product similarity between patch tokens:

$$S_{m \rightarrow a} = \frac{f_{1:P}^{(m)} (f_{1:P}^{(a)})^\top}{\sqrt{d}} \in \mathbb{R}^{P \times P}, \quad \mathbf{A}_{m \rightarrow a}^{\text{pred}} = \sigma(S_{m \rightarrow a}) \in (0, 1)^{P \times P}, \quad (1)$$

where each row encodes which auxiliary patches correspond to a given main-view patch, allowing one-to-many matches.

Supervision and auxiliary objectives. We train ACM with three losses. We supervise $S_{m \rightarrow a}$ with the sparse geometry-derived matrix $A_{m \rightarrow a}^{\text{gt}}$ using a focal BCE with logits to address extreme class imbalance. In addition, we apply an auxiliary row-wise cross-entropy on the patch-to-patch correspondence logits, i.e., $Z_{m \rightarrow a}^{\text{patch}} = Z_{m \rightarrow a}[1:P, 1:P]$ (excluding the [CLS] token). The target distribution is obtained by normalizing each positive row of A^{gt} , and rows with no positives are ignored. We average both directions:

$$\mathcal{L}_{\text{attn}} = \frac{1}{2} \left(\text{CE}_{\text{row}}(Z_{m \rightarrow a}^{\text{patch}}, A_{m \rightarrow a}^{\text{gt}}) + \text{CE}_{\text{row}}(Z_{a \rightarrow m}^{\text{patch}}, (A_{m \rightarrow a}^{\text{gt}})^\top) \right). \quad (2)$$

Finally, we include a negative-mass penalty that discourages high average predicted probability on non-corresponding entries:

$$\mathcal{L}_{\text{neg}} = \frac{1}{|\Omega^-|} \sum_{(i,j) \in \Omega^-} \sigma(S_{m \rightarrow a}[i,j])^\rho, \quad \Omega^- = \{(i,j) \mid A_{m \rightarrow a}^{\text{gt}}[i,j] = 0\}, \quad (3)$$

with exponent ρ . The overall objective is

$$\mathcal{L}_{ac} = \mathcal{L}_{\text{focal}} + \lambda_{\text{attn}} \mathcal{L}_{\text{attn}} + \lambda_{\text{neg}} \mathcal{L}_{\text{neg}}, \quad (4)$$

2.4 Anatomy-Correspondence Fusion and Reporting

Anatomy-Correspondence Fusion. MAC-XA first aligns each auxiliary view to the main-view patch coordinate space and then aggregates the aligned evidence for report generation. For each main-aux pair, we apply ACM to obtain mapped tokens \bar{f} and convert the similarity logits $S_{m \rightarrow a}$ in Eq. (1) into row-normalized alignment weights $W_{m \rightarrow a}$ via a softmax. We then align auxiliary *raw* patch tokens as $\tilde{f}_{1:P}^{(a)} = W_{m \rightarrow a} f_{1:P}^{(a)}$ and define the mapping update as $\Delta^{(m)} = \bar{f}^{(m)} - f^{(m)}$. Using token-wise gates g_{raw} and g_{map} , we update only the patch tokens:

$$f_{1:P}^{(m)} \leftarrow f_{1:P}^{(m)} + g_{\text{raw},1:P} \odot \tilde{f}_{1:P}^{(a)} + g_{\text{map},1:P} \odot \Delta_{1:P}^{(m)}. \quad (5)$$

For a multi-view sample, we randomly select one main view and $K \in \{1, 2, 3\}$ auxiliary views, and apply Eq. (5) sequentially over auxiliaries to obtain fused tokens f^{fusion} .

Structured Stenosis Reporting Head. We attach a lightweight projection head that maps f^{fusion} to the language-model embedding space and use a cross-attention decoder (DistilGPT2 [16]) to generate reports under a fixed template and controlled vocabulary. Training uses token-level cross entropy, with optional lexical reweighting following the lexical weighted loss in [19], where we upweight clinically critical tokens specific to coronary stenosis reporting, mainly branch names and stenosis severity levels.

2.5 Implementation Details

We synthesize 68,096 DRR angiograms from 38 patients (9,728 simulated cases; 8 LCA and 6 RCA views) and use a patient-wise split of 32/3/3 for training, validation, and testing. We pretrain ACM with AdamW using a learning rate and weight decay of 1×10^{-4} . The training objective combines focal BCE ($\alpha = 0.75$, $\gamma = 2.0$), attention CE ($\lambda_{\text{attn}} = 0.05$), and negative-mass regularization ($\lambda_{\text{neg}} = 0.05$, $\rho = 1.0$), with the latter two terms linearly warmed up. For reporting, we fuse one main view with $K \in \{1, 2, 3\}$ auxiliary views (random during training and deterministic during evaluation) and optimize only the decoder, projection head, and fusion gates with AdamW at a learning rate of 1×10^{-4} .

3 Experiments and Results

3.1 Dataset and Evaluation Metrics

For external verification, we use the public multi-view coronary angiography dataset released by Mahmoudi *et al.* [12]. The release provides angiograms together with a per-case SYNTAX-info dictionary, from which we parse lesion location and stenosis severity and convert them into our structured report template. An experienced clinician applies predefined eligibility criteria to identify 50 evaluable cases, requiring an interpretable SYNTAX-info record, cross-view consistency within the same coronary system, and sufficient vessel visibility across views. Studies with corrupted metadata, mismatched coronary systems across views, severe device occlusion, or major image-quality limitations are excluded.

To assess correspondence quality where ground-truth correspondences are available, we measure the agreement between the predicted correspondence confidence map $A^{\text{pred}} \in [0, 1]^{P \times P}$ and a sparse binary correspondence matrix $A^{\text{gt}} \in \{0, 1\}^{P \times P}$ using Soft-Dice, IoU@Top- k , and AUPRC; on real cases without A^{gt} , we rely on clinician review of correspondence correctness. For report generation, we report natural language generation (NLG) metrics (CIDEr, ROUGE-L (R-L)) and template-aware structured metrics by parsing each lesion entry into $I = (b, c, g, p)$ (branch name, count, severity grade, percent stenosis): $F1_b$ requires exact segment-level matching (correct branch *and* SYNTAX-defined sub-segment), $F1_s$ evaluates branch correctness under a coarser grouping that ignores within-branch sub-segments, $F1_{bn}$ measures stenosis-count consistency on matched branches, and Sev. measures severity agreement on BN-matched items.

Table 1: Single-view baseline scores (in %) on synthetic and real datasets.

Setting	Clinical (Abs.)				NLG (Abs.)	
	F1 _b ↑	F1 _{bn} ↑	F1 _s ↑	Sev. ↑	CIDEr ↑	R-L ↑
Single-view (Syn)	59.46	31.11	72.31	51.71	58.90	61.97
Single-view (Real)	26.16	23.51	45.18	45.80	6.49	41.39

Table 2: Synthetic report generation results: attention-AC-GT alignment (Abs., in %) and improvements (Δ , in %) over the single-view baseline; see Table 1.

Method	Align (Abs.)			Clinical (Δ)				NLG (Δ)	
	sDice ↑	IoU@k ↑	AUPRC ↑	F1 _b ↑	F1 _{bn} ↑	F1 _s ↑	Sev ↑	CIDEr ↑	R-L ↑
MeanPool	–	–	–	-2.18	-2.89	+0.39	-0.58	+2.92	+1.01
ConcatTok	–	–	–	-1.45	+0.91	-2.04	-2.84	-2.65	-0.33
DuoDuo	0.09	1.20	4.53	-4.79	-3.36	-5.11	+0.51	-11.13	-3.06
CrossAttn	0.18	0.72	3.66	-2.69	-0.88	-0.15	-2.45	+5.39	+1.71
Ours	23.08	35.32	53.34	+6.11	+3.60	+7.03	+2.57	+9.44	+1.39

For reference, Table 1 reports the absolute single-view baseline scores on both synthetic and real data; all subsequent result tables report improvements Δ over this baseline unless stated otherwise.

3.2 Evaluation on Synthetic Data

We evaluate correspondence quality and downstream reporting jointly on synthetic data (Table 2). Our comparison includes attention-based baselines, *Cross-Attention* (CrossAttn) and *Duoduo-style Multi-view Attention* (DuoDuo) [8], as well as simple fusion variants (MeanPool, ConcatTok). For fair comparison, all methods use identical frozen RAD-DINO features and the same pretrained PoseViT priors, and differ only in the fusion module. We report the agreement between the predicted correspondence map and AC-GT as absolute scores in the Align (Abs.) columns, and report-generation gains as Δ over the single-view baseline on clinical and NLG metrics. Our method achieves higher alignment with geometry-derived correspondences and yields the best improvements in structured correctness, indicating that accurate, inspectable correspondences enable more reliable multi-view evidence aggregation.

3.3 Zero-shot Real Transfer on 50 Patients

We evaluate zero-shot transfer by applying models trained on synthetic data to a 50-case real multi-view cohort without further adaptation. Two aspects are assessed. First, we examine bidirectional cross-view correspondence with clinician evaluation. For each case, a stenotic patch in view A is used to predict its correspondence in view B, followed by the reverse direction ($A \rightarrow B$ and $B \rightarrow A$), yielding 100 samples. Two experienced clinicians reached consensus that 87/100 predictions were accurately localized. In contrast, CrossAttn and DuoDuo produced diffuse heatmaps with limited anatomical specificity, often highlighting

Table 3: Real report generation results: improvements (Δ , in %) over the single-view baseline, see Table 1.

Method	Clinical (Δ)				NLG (Δ)	
	F1 _b \uparrow	F1 _{bn} \uparrow	F1 _s \uparrow	Sev. \uparrow	CIDEr \uparrow	R-L \uparrow
MeanPool	+4.99	+1.66	+1.67	+10.67	-1.36	+2.36
ConcatTok	-0.69	+4.93	-1.43	+11.60	-4.86	+2.68
DuoDuo	+3.97	+3.62	+1.51	+8.40	-2.13	+4.70
CrossAttn	+3.24	+2.79	+1.33	+10.17	-4.13	+2.87
Ours	+10.19	+11.23	+10.14	+22.57	+2.01	+6.20

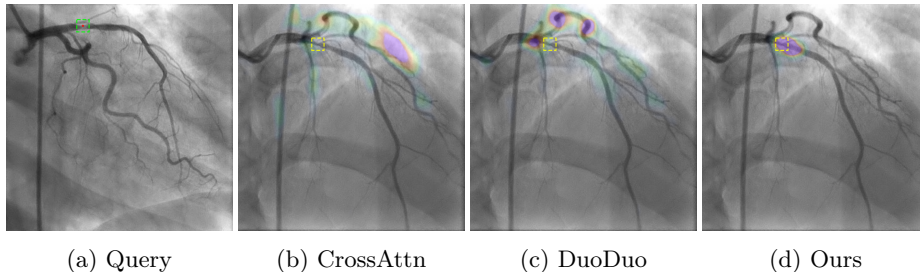


Fig. 2: Cross-view correspondence prediction on real angiograms. (a) Reference view with a query patch centered on the stenotic region (green dashed box). (b–d) Predicted correspondence heatmaps on the second view with the manually labeled ground-truth correspondence patch (yellow dashed box).

broad vessel regions rather than precise correspondences (Fig. 2). Second, we evaluate zero-shot report generation on the same cohort (Table 3). Together, these results demonstrate effective correspondence transfer and improved structured reporting under a clinically realistic, no-adaptation setting.

4 Discussion and Conclusion

Interestingly, several multi-view baselines show negative relative gains on synthetic data but positive improvements when transferred zero-shot to real angiograms. We attribute this discrepancy to differences in distribution complexity and information redundancy. The synthetic dataset is generated under controlled conditions with limited noise, minimal occlusion, and stable projection geometry, where single-view inputs already provide sufficient evidence for stenosis assessment. In this regime, naïve multi-view fusion may introduce redundant information or minor misalignment noise, leading to marginal degradation. In contrast, real-world angiography involves incomplete contrast filling, device occlusion, vessel overlap, and projection distortion, making single-view evidence unstable or incomplete. Here, multi-view aggregation becomes beneficial by reducing prediction variance and recovering complementary anatomical cues.

In conclusion, MAC-XA formulates multi-view coronary report generation as an alignment-constrained aggregation problem and shows that geometry-supervised anatomical correspondence learning is key to robust cross-view reasoning. The synthetic dataset plays a critical role by providing controllable, geometry-derived correspondence supervision unavailable in real data, enabling principled pretraining. Together, these findings demonstrate that anatomically grounded alignment, supported by synthetic supervision, is essential for reliable and generalizable multi-view stenosis reporting in clinical practice.

References

1. Ahmadi, A., Argulian, E., Leipsic, J., Newby, D.E., Narula, J.: From subclinical atherosclerosis to plaque progression and acute coronary events: Jacc state-of-the-art review. *Journal of the American College of Cardiology* **74**(12), 1608–1617 (2019)
2. Bai, Q., Zou, X., Alhaskawi, A., Dong, Y., Zhou, H., Ezzi, S.H.A., Kota, V.G., AbdullaAbdulla, M.H.H., Abdalbary, S.A., Hu, X., Lu, H.: Multi-view contrastive learning and symptom extraction insights for medical report generation. *Scientific Reports* **15**(1) (May 2025)
3. Chen, S.J., Carroll, J.D.: 3-d reconstruction of coronary arterial tree to optimize angiographic visualization. *IEEE transactions on medical imaging* **19**(4), 318–336 (2000)
4. Gharleghi, R., Adikari, D., Ellenberger, K., Ooi, S.Y., Ellis, C., Chen, C.M., Gao, R., He, Y., Hussain, R., Lee, C.Y., et al.: Automated segmentation of normal and diseased coronary arteries—the asoca challenge. *Computerized Medical Imaging and Graphics* **97**, 102049 (2022)
5. Ghobrial, M., Haley, H.A., Gosling, R., Rammohan, V., Lawford, P.V., Hose, D.R., Gunn, J.P., Morris, P.D.: The new role of diagnostic angiography in coronary physiological assessment. *Heart* **107**(10), 783–789 (2021)
6. Green, N.E., Chen, S.Y.J., Hansgen, A.R., Messenger, J.C., Groves, B.M., Carroll, J.D.: Angiographic views used for percutaneous coronary interventions: A three-dimensional analysis of physician-determined vs. computer-generated views. *Catheterization and Cardiovascular Interventions* **64**(4), 451–459 (2005)
7. Kočka, V., Thériault-Lauzier, P., Xiong, T.Y., Ben-Shoshan, J., Petr, R., Laboš, M., Buithieu, J., Mousavi, N., Pilgrim, T., Praz, F., et al.: Optimal fluoroscopic projections of coronary ostia and bifurcations defined by computed tomographic coronary angiography. *Cardiovascular Interventions* **13**(21), 2560–2570 (2020)
8. Lee, H.H., Zhang, Y., Chang, A.X.: Duoduo clip: Efficient 3d understanding with multi-view images. In: *The Thirteenth International Conference on Learning Representations* (2025)
9. Lee, J.B., Chang, S.G., Kim, S.Y., Lee, Y.S., Ryu, J.K., Choi, J.Y., Kim, K.S., Park, J.S.: Assessment of three dimensional quantitative coronary analysis by using rotational angiography for measurement of vessel length and diameter. *The International Journal of Cardiovascular Imaging* **28**(7), 1627–1634 (2012)
10. Liu, K., Ma, Z., Kang, X., Li, Y., Xie, K., Jiao, Z., Miao, Q.: Enhanced contrastive learning with multi-view longitudinal data for chest x-ray report generation. In: *Proceedings of the Computer Vision and Pattern Recognition Conference*. pp. 10348–10359 (2025)

11. Liu, Z., Zhu, Z., Zheng, S., Zhao, Y., He, K., Zhao, Y.: From observation to concept: A flexible multi-view paradigm for medical report generation. *IEEE Transactions on Multimedia* **26**, 5987–5995 (2023)
12. Mahmoudi, S.S., Alishani, M.M., Emdadi, M., Hosseiniyan Khatibi, S.M., Khodaei, B., Ghaffari, A., Oskui, S.D., Ghaffari, S., Pirmoradi, S.: X-ray coronary angiogram images and syntax score to develop machine-learning algorithms for chd diagnosis. *Scientific Data* **12**(1), 471 (2025)
13. Mensah, G.A., Fuster, V., Roth, G.A.: A heart-healthy and stroke-free world: using data to inform global action (2023)
14. Pérez-García, F., Sharma, H., Bond-Taylor, S., Bouzid, K., Salvatelli, V., Ilse, M., Bannur, S., Castro, D.C., Schwaighofer, A., Lungren, M.P., et al.: Exploring scalable medical image encoders beyond text supervision. *Nature Machine Intelligence* **7**(1), 119–130 (2025)
15. Preuhs, A., Berger, M., Bauer, S., Redel, T., Unberath, M., Achenbach, S., Maier, A.: Viewpoint planning for quantitative coronary angiography. *International Journal of Computer Assisted Radiology and Surgery* **13**(8), 1159–1167 (2018)
16. Radford, A., Wu, J., Child, R., Luan, D., Amodei, D., Sutskever, I., et al.: Language models are unsupervised multitask learners. *OpenAI blog* **1**(8), 9 (2019)
17. Sianos, G., Morel, M.A., Kappetein, A.P., Morice, M.C., Colombo, A., Dawkins, K., Van Den Brand, M., Van Dyck, N., Russell, M.E., Mohr, F.W., et al.: The syntax score: an angiographic tool grading the complexity of coronary artery disease. *EuroIntervention* **1**(2), 219–227 (2005)
18. Tu, S., Hao, P., Koning, G., Wei, X., Song, X., Chen, A., Reiber, J.: In vivo assessment of optimal viewing angles from x-ray coronary angiography. *EuroIntervention* **7**(1), 112–120 (2011)
19. Zhang, B., Jia, C., Liu, S., Schunkert, H., Navab, N.: Semantic-aware chest x-ray report generation with domain-specific lexicon and diversity-controlled retrieval. In: *International Conference on Medical Image Computing and Computer-Assisted Intervention*. pp. 607–616. Springer (2025)
20. Zhang, B., Zhang, Z., Liu, S., Faghihroohi, S., Schunkert, H., Navab, N.: Xa-sim2real: adaptive representation learning for vessel segmentation in x-ray angiography. In: *International Conference on Medical Image Computing and Computer-Assisted Intervention*. pp. 747–756. Springer (2024)